Effects of organophilic-modified attapulgite nanorods on thermal and mechanical behavior of segmented polyurethane elastomers

Chia-Hao Wang[1], Yeong-Tarng Shieh[2], Gangjian Guo[1], Steven Nutt[1]

1. M.C. Gill Composites Center, Mork Family Department of Chemical Engineering and Materials Science, University of Southern California, Los Angeles 90089-0241
2. Department of Chemical and Materials Engineering, National University of Kaohsiung, Kaohsiung 811, Taiwan

Abstract: The effects of different grafting content of 4,4′-methlenebis(phenyl isocyanate)-modified attapulgite (ATT-MDI) on thermal and mechanical properties of segmented polyurethane (PU) elastomers were investigated. The ATT-MDI nanorods with different grafting content were prepared by treating ATT with heat and acid followed by grafting with MDI molecules. MDI-modified ATT were characterized by transmission electron microscopy (TEM), thermogravimetric analysis (TGA), and Fourier transform infrared spectroscopy. TGA analysis revealed that at least 30 wt % of MDI was grafted/adsorbed on the surface of ATT following the modification. Three PU/ATT-MDI nanocomposites were in situ synthesized using ATT with different grafting contents, and the materials were characterized by TEM, thermal analysis, and mechanical testing. The tensile strength and modulus increased with increasing grafting content of MDI molecules, and the crystallinity of soft and hard segments was increased by ATT-MDI.

1. Introduction

Since organic–inorganic nanocomposites based on layered silicates were first introduced by Toyota Research Center (combining nylon and montmorillonite) [1–3], inorganic nanofillers have been

Please cite this article as: M. Wong, R. Tsuji, H.J. Sue, and S. Nutt; **Glass transition temperature changes of polymer nanocomposites comprised of finely dispersed ZnO quantum dots**, Soft Matter 6 (2010) 4482-4490, DOI: http://dx.doi.org/10.1039/b927182a

widely studied, creating the field of polymer/inorganic nanocomposites [4–7]. For example, the introduction of small amount of nanofillers has been shown to cause increases in strength, stiffness, and heat resistance of polymers [8–12]. However, the major drawbacks for inorganic nanofillers are poor dispersion in polymer resins and weak interfacial adhesion with polymer matrices. Surface modification by grafting organic molecules onto nanoscale inorganic silicates offers an effective method to improve the dispersion in polymer matrices and increase the interfacial adhesion between inorganic nanofillers and polymer networks. In other words, organically modified nanofillers prevent aggregation and increase affinity with polymer matrices.

Segmented polyurethane (PU) elastomer is widely used in commercial applications. Its attributes include high abrasion resistance, shock absorption, flexibility, elasticity, and resistance to chemicals [13]. These properties originate primarily from the tendency of PU to form discrete regions of microdomains. The linear chain structure of PU can be expressed in the form of (A–B)n, where the hard segment A is composed of low-molecular weight diol or diamine (chain extender) with diisocyanate, and the soft segment B is composed of high-molecular weight polyester or polyether polyol. Because of the different chemical structure of the hard and soft segments, repulsive interactions and thermodynamic incompatibility lead to microphase segregation [14], and formation of hard and soft segment domain aluminosilicates. The hard segments segregate into a glassy or microcrystalline domain, and the soft segments form rubbery matrices in which the hard segments are dispersed [15].

Attapulgite (ATT) is a hydrated magnesium aluminosilicate with chemical formula $[(Mg, Al, Fe)_5Si_8O_{20}(OH)_2(OH_2)_4]\cdot 4H_2O$ [16]. Although ATT features ribbons of a 2:1 phyllosilicate structure, it differs from other layered silicates in that it lacks continuous octahedral sheets. Each ribbon is linked to the next by inversion of SiO4 tetrahedra along a set of Si-O-Si bonds which

extend parallel to the x-axis, forming rectangular channels that contain zeolitic water [17]. The average external and internal surface areas have been estimated to be 300 and 600 m2/g, respectively [17]. Because of the unique morphology and structure, ATT has been used for various commercial applications, such as adsorbents, catalysts, rheological agents, and fillers [17–21].

Researchers have studied the heat treatment [22–27] and acid treatment of ATT [28–32]. These treatments are commonly used to increase surface area and enhance active sites for ATT, although the combination of heat and acid treatment has rarely been considered. Additional surface modification is accomplished through coupling agents, which only are grafted onto the inorganic silicate surface and reacts with polymer chains. The idea to use diisocyanate molecule as a coupling agent on silicates surface via reaction with silanol groups (Si-OH) was first introduced by Yosomiya et al. [33], who grafted various diisocyanate compounds via silanol groups onto the glass fiber. Their work indicated that the silanol group (Si-OH) had reactivity similar to alcohol (OH) when reacted with diisocyanate, and attributed this to a comparable activation energy. In a previous study, ATT was organically modified to achieve significant improvements in the mechanical and thermal properties of PU elastomers [34]. However, the measured amounts of organic molecules grafted onto ATT were much lower than the amounts predicted by theoretical calculations. To enhance the efficiency of grafting organic molecules on the surface of ATT, different treatments were conducted using a design of experiments approach. In this work, we use heat and acid treatments to form Si-OH groups on ATT followed by grafting MDI to investigate the effects of different grafting contents on thermal and mechanical properties of the in situ synthesized PU/ATT-MDI nanocomposites.

2. Experimental

2.1Materials

ATT (Attagel 50, Engelhard Co., USA) was selected for experiments and used as received. The diisocyanate, MDI (98%, Sigma-Aldrich), was purified by filtration of molten MDI liquid at 70°C. Dibutyltin dilaurate (95%, Sigma-Aldrich) was used as a catalyst for grafting MDI molecules on the surface of ATT. PU and PU/ATT-MDI nanocomposites were prepared using 1,4-butanediol (BDO, Avocado Research Chemicals) and polytetrahydrofuran (PTHF, Sigma-Aldrich, Mw 2,900), which are the hydroxyl terminated monomer and oligomer, respectively. The 1,4-BDO was dried over calcium hydride for 48 h and then was vacuum distilled. Polytetrahydrofuran was dehydrated in a vacuum oven at 60°C for 48 h. Dimethylformamide (DMF, Sigma-Aldrich) was dehydrated and used as a solvent in the polymerization reaction.

2.2 Synthesis of PU Elastomer and PU/ATT-MDI Nanocomposites

PU elastomer was synthesized with a molar ratio of 4:1:2.64 (MDI-to-PTHF-to-1,4BDO), using excess diisocyanate to produce partially crosslinked networks and [BOND]NCO end groups [35]. First, the oligomeric polyol (PTHF) was dissolved in DMF and reacted with MDI at 80°C for 30 min to obtain a prepolymer in a round bottom flask with continuous stirring under vacuum. Second, the chain extender (1,4-BDO) was added to build up the PU network, and the mixture was allowed to react at 80°C for an additional 2 min. In initial experiments, the network building reaction was active within 2 min (after the addition of 1,4-BDO). If the reaction was allowed to continue beyond 2 min, the viscosity increased rapidly, making it impossible to pour out of the round bottom flask.

Finally, the mixture was poured into a Teflon® mold and cured at 80°C for 24 h to obtain the PU elastomers. To prevent moisture absorption, the reaction was performed under vacuum, and all chemicals were dehydrated beforehand.

Three different grafting amounts of ATT-MDI nanorods (ATT-MDI-H500A1M1H, ATT-MDI-H600A5M4H, and ATT-MDI-H700A3M2H), were chosen to synthesize the PU/ATT-MDI nanocomposites, representing high-, medium-, and low-grafting contents, respectively. The PU/ATT-MDI nancomposites were prepared with 2.5 wt % ATT-MDI loading in identical molar ratios. Figure 1 illustrates the steps in the synthesis route and the associated chemical structures. First, the ATT-MDI nanorods were directly blended with polytetrahydrofuran (PTHF), which was dissolved in the DMF solvent using a high-speed dual-axis mixer (HM-500, Keyence, USA) for 30 min to form OH-terminated urethane oligomers. Second, excess MDI was added to the mixture, forming the prepolymer at 80°C under vacuum for 30 min. Subsequently, the chain extender 1,4-BDO was added to the prepolymer with vigorous stirring for 2 min to complete the reaction. Finally, the viscous polymer was poured into a Teflon® mold and cured at 80°C for 24 h to form PU/ATT-MDI nanocomposites. The three samples will be referred to as PU/ATT-MDI-H500A1M1H, PU/ATT-MDI-H600A5M4H, and PU/ATT-MDI-H700A3M2H, respectively.

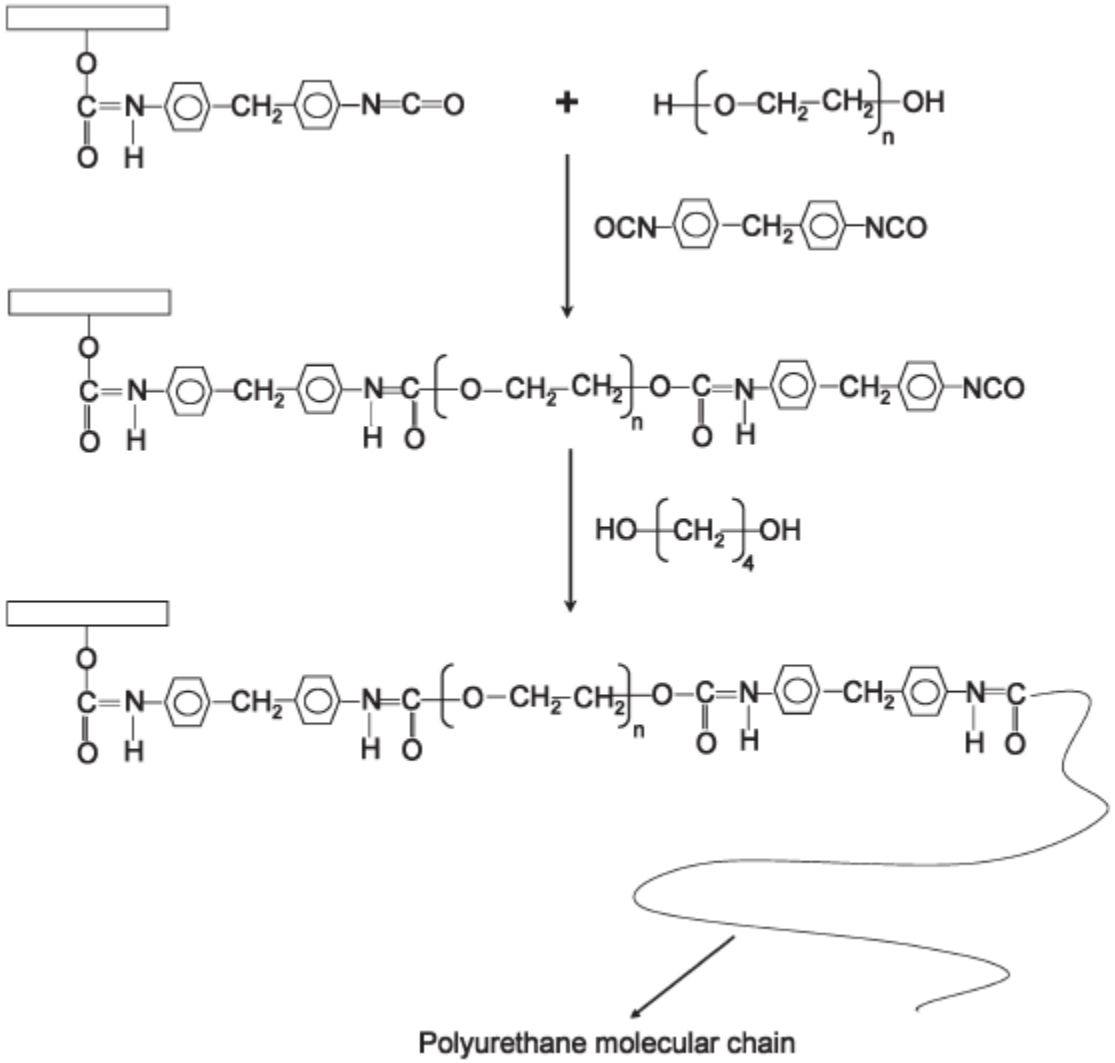

Figure 1: *Synthesis of PU/ATT-MDI nanocomposite.*

2.3 Characterization

Thermogravimetric analysis (TGA 2050, TA Instruments) was performed to determine the amount of diisocyanate grafted on the surface of ATT nanorods. Samples were heated to 800°C at 10°C/min under nitrogen flow.

Fourier transform infrared (FTIR) spectroscopy (Nicolet 4700) with a sensitivity of 128 scans and a resolution of 4 cm−1 was performed on the untreated ATT, heat- and acid-treated ATT (ATT-OH),

Please cite this article as: M. Wong, R. Tsuji, H.J. Sue, and S. Nutt; **Glass transition temperature changes of polymer nanocomposites comprised of finely dispersed ZnO quantum dots**, Soft Matter 6 (2010) 4482-4490, DOI: http://dx.doi.org/10.1039/b927182a

and grafted ATT (ATT-MDI), respectively. KBr/ATT disks were prepared and used to obtain the IR spectra.

The morphology of untreated ATT and the heat- and acid-treated ATT nanorods were observed by transmission electron microscopy (TEM Philips EM420). The TEM samples were prepared using gentle sonication in deionized water to create a colloidal suspension. A drop of the colloidal was placed on the grid with dry analyzed at an acceleration voltage of 120 kV. The dispersion of the ATT-MDI nanorods in the PU matrix was also observed with ultrathin samples, which were sectioned by cryogenic ultra-microtoming.

The melting temperatures of the soft and hard segments in PU and PU/ATT-MDI nanocomposites were measured by differential scanning calorimetry (DSC 2920, TA Instruments). Measurements were performed by scanning twice to avoid signal noise and to erase thermal history. In the first scan, the sample was heated to 250° (at 10°/min), then cooled to −65°C. In the second scan, the sample was heated to 300°C at a heating rate of 10°/min. The second scan was used to record transition temperatures.

The storage modulus (G′) was assessed by dynamic mechanical thermal analysis (DMTA Q800, TA Instruments). Tests were conducted using the temperature scan mode, from −100 to 250°C, at a 10°/min heating rate. The frequency of the forced oscillations was set to 1 Hz and the applied deformation was 0.05%.

Tensile strength, modulus, and elongation at break were measured using a universal testing machine (Instron 8531). Tests were performed on dog-bone shaped specimens using a crosshead speed of 10 mm/min at room temperature, in accordance with ASTM D 638-94b.

3. Results and Discussions

3.1 Characterization of ATT

The fibrous morphology of untreated and treated ATT were revealed by TEM (Fig. 2). In the untreated condition (Fig. 2a), the fibers were rod-shaped and formed a randomly oriented, densely packed network. The ATT nanorods were ~15–25 nm in diameter and 0.2 to several microns in length. The high-aspect ratio (length-to-diameter) resulted in high-specific surface area to interact with the continuous polymeric matrix. After heat and acid treatment, the external morphology of ATT was preserved (Fig. 2b), although rough surface with pits was evident in the ATT nanorods. The persistence of the fibrous morphology indirectly shows that the heat and acid treatment affected structure throughout the internal microchannels.

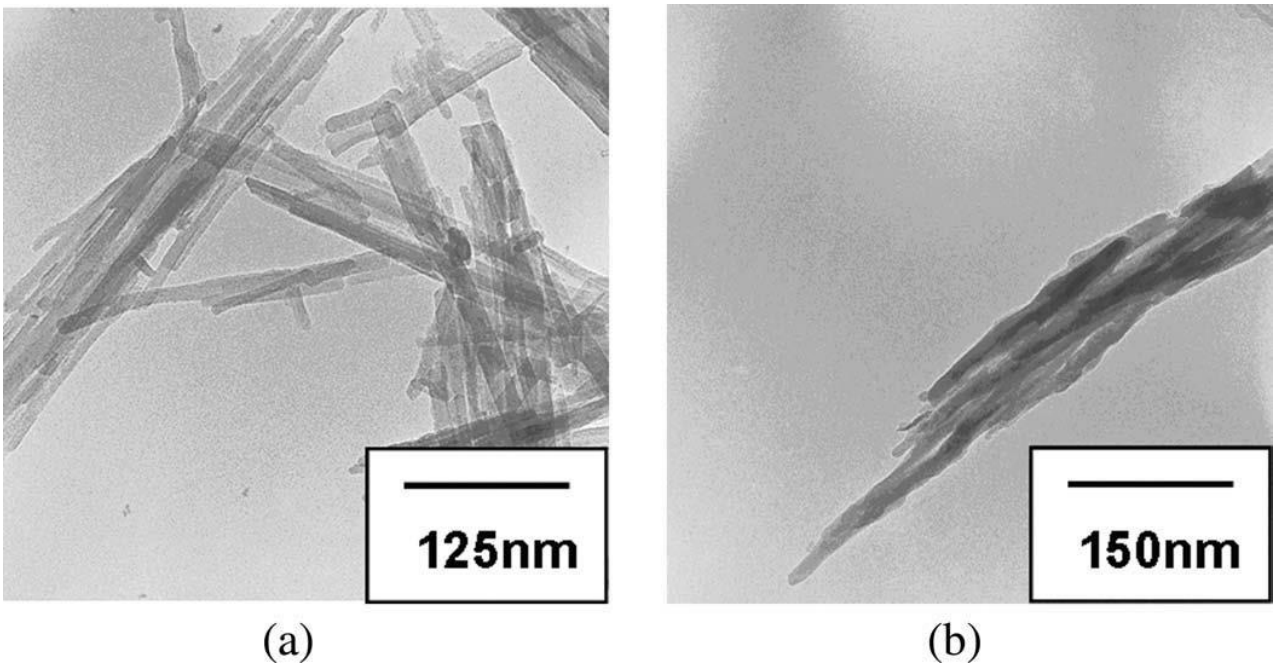

Figure 2: *TEM images for (a) untreated ATT and (b) heat and acid-treated ATT.*

Figure 3 shows two thermogravimetric curves—one for pristine ATT after heat (500°C) and acid (1 M HCl for 1h) treatment (ATT-OH), and one for MDI-grafted ATT (ATT-MDI). The mass loss of the ATT-OH below 120°C is attributed to evaporation of a small amount of adsorbed moisture. Below 120°C, the MDI-grafted ATT curve shows much less weight loss than the heat- and acid-treated ATT. The ATT-MDI had become hydrophobic clay and consequently adsorbed less moisture than ATT-OH. Discounting the mass loss of ATT-OH, the mass fraction of organic groups eliminated at 600°C was approximately 52 wt % for ATT-MDI. The mass fraction lost indicates that the two-step surface modification process led to a significant mass fraction of organic groups bonded to ATT. After the TGA measurement, the content of the grafted diisocyanate on the surface of ATT nanorods based on DOE was measured, as summarized in Table 1. H500A1M1H exhibited the maximum amount of MDI grafting, while H700A3M2H exhibited the minimum amount of MDI grafting. The difference between two samples in the amount of MDI grafting was more than 20 wt %, and was attributed to changes in the structure and composition in ATT after the heat and acid treatment.

Table 1: *Grafting amount of MDI as obtained from TGA heating at 20°C/min under N2 to 600°C*

ATT-OH samples	**Weight loss (wt%)**	**ATT-MDI samples**	**Weight loss (wt%)**	**Grafting amount of MDI (wt%)**
H500A1M1H	88.99	H500A1M1H	36.98	52.01
H500A1M1H	89.02	H500A1M1H	37.16	51.86
H500A5M4H	89.30	H500A5M4H	43.36	45.94
H500A5M8H	91.41	H500A5M8H	52.08	39.33
H500A9M1H	91.45	H500A9M1H	52.34	39.11

ATT-OH samples	Weight loss (wt%)	ATT-MDI samples	Weight loss (wt%)	Grafting amount of MDI (wt%)
H500A9M8H	91.84	H500A9M8H	54.57	37.27
H600A3M6H	91.08	H600A3M6H	48.44	42.64
H600A5M4H	92.13	H600A5M4H	46.61	45.52
H600A5M4H	91.57	H600A5M4H	46.31	45.26
H600A9M4H	92.14	H600A9M4H	49.40	42.74
H700A3M2H	90.62	H700A3M2H	59.91	30.71
H800A1M4H	93.88	H800A1M4H	42.36	51.52
H800A1M8H	92.79	H800A1M8H	47.94	44.85
H800A5M1H	92.90	H800A5M1H	43.39	49.51
H800A5M8H	92.65	H800A5M8H	44.61	48.04
H800A9M4H	91.67	H800A9M4H	43.13	48.54
H800A9M4H	91.53	H800A9M4H	43.36	48.17

Please cite this article as: M. Wong, R. Tsuji, H.J. Sue, and S. Nutt; **Glass transition temperature changes of polymer nanocomposites comprised of finely dispersed ZnO quantum dots**, Soft Matter 6 (2010) 4482-4490, DOI: http://dx.doi.org/10.1039/b927182a

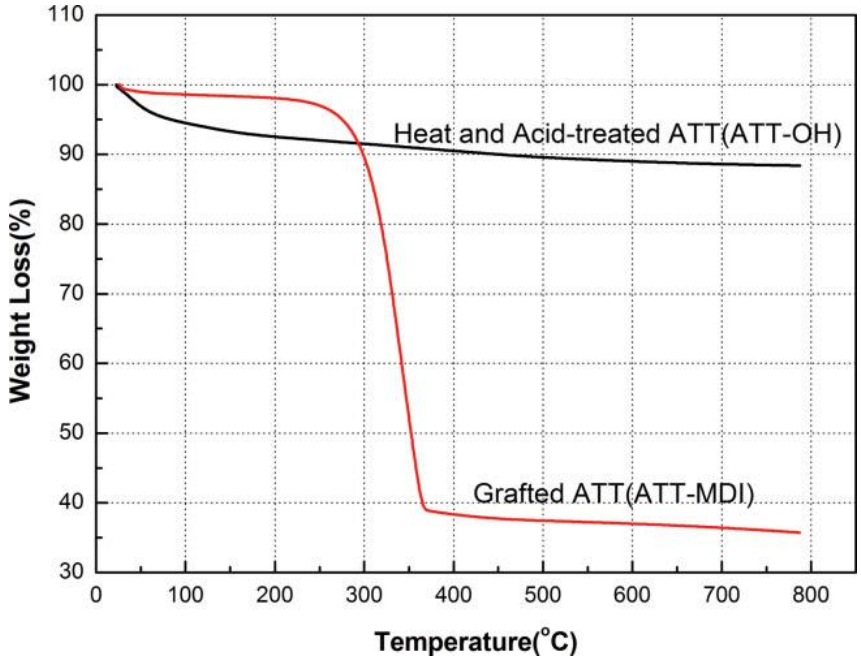

Figure 3: *TEM images for (a) untreated ATT and (b) heat and acid-treated ATT.*

The FTIR spectrum of the untreated ATT, H700A3M2H ATT-OH, and H700A3M2H ATT-MDI (which had the minimum amount of MDI grafting) are shown in Fig. 4. In the high-wavenumber region (3700–3200 cm−1), the untreated ATT (Fig. 4a) revealed two characteristic absorption bands at 3615 and 3548 cm−1, and two shoulders at 3400–3420 and 3260–3290 cm−1. The first two bands were assigned to Al3+-OH and (Fe3+, Mg)-OH, while the two shoulders were attributed to hydrogen bound to oxygen in Si-O-Si and Si-O-Al groups, respectively [36]. After heat and acid treatment, the high-wavenumber region became broad and the band that appeared at 1655 cm−1 in untreated ATT shifted to 1636 cm−1 with decreased intensity. Mendelovici suggested that this shift was related to energetically different hydrogen bondings [28]. In addition, after the heat and acid treatment, the absorption band at 878 cm−1 disappeared, and a new shoulder appeared at 960–955 cm−1. Also, the three absorptions at 985, 1031, and 1195 cm−1 were merged into one characteristic

Please cite this article as: M. Wong, R. Tsuji, H.J. Sue, and S. Nutt; **Glass transition temperature changes of polymer nanocomposites comprised of finely dispersed ZnO quantum dots**, Soft Matter 6 (2010) 4482-4490, DOI: http://dx.doi.org/10.1039/b927182a

band at 1072 cm−1. The new shoulder signified that new silanol groups (Si-OH) had formed and the merged band indicated that the ATT crystal structure had been modified.

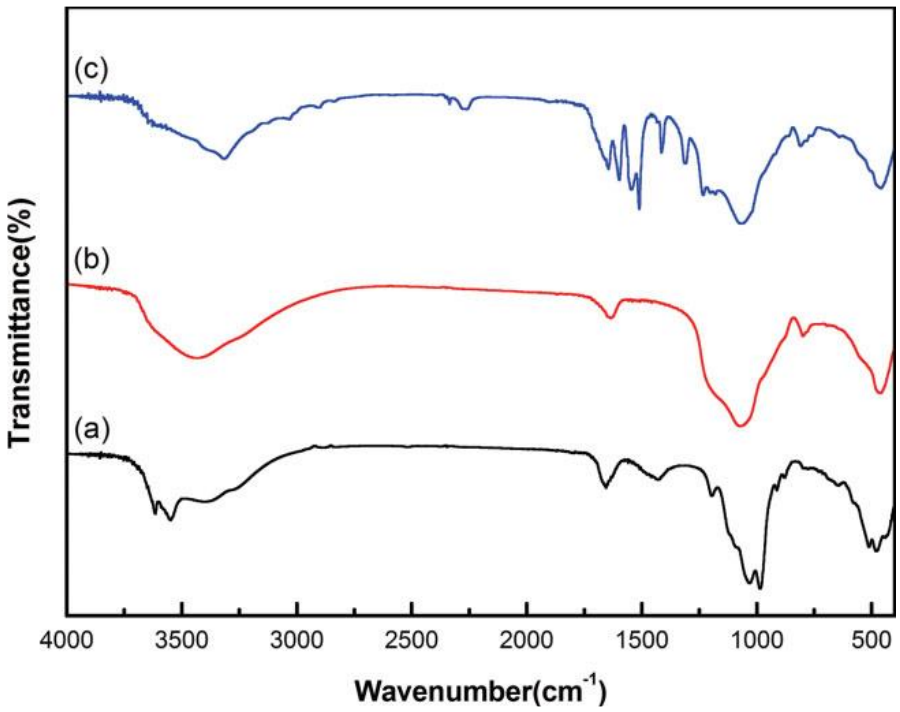

Figure 4: *TEM images for (a) untreated ATT and (b) heat and acid-treated ATT.*

Two of the main regions of interest in the spectrum of H700A3M2H ATT-MDI are the NH absorption and C-O stretching. The NH absorption peak at 3316 cm−1, can be attributed to hydrogen-bonded NH groups of urethane linkages [37], while the small shoulder at 3420 cm−1 is characteristic of stretching of free NH groups. Moreover, the broad band arising from adsorbed water in the high-wavenumber region is absent (Fig. 4c), indicating that the hydrophilic character of the ATT-MDI strongly decreased. On the other hand, the absorbance due to stretching of NCO groups at 2275 cm−1 [37] is clearly visible. The amide bands at 1645, 1511, and 1309cm−1, assigned to CO (Amide I), NH (Amide II), and CNH (Amide III), respectively, are also clearly observed and are consistent with polyurea formation [37–39]. These results indicate that the MDI molecules were

Please cite this article as: M. Wong, R. Tsuji, H.J. Sue, and S. Nutt; **Glass transition temperature changes of polymer nanocomposites comprised of finely dispersed ZnO quantum dots**, Soft Matter 6 (2010) 4482-4490, DOI: http://dx.doi.org/10.1039/b927182a

grafted onto the ATT surface through chemical bonding even in the H700A3M2H ATT-MDI, which had the lowest grafting amount.

3.2PU/ATT-MDI Nanocomposites

3.2.1 Morphology of PU/ATT-MDI Nanocomposites

The morphology of PU/ATT-MDI-H500A1M1H, PU/ATT-MDI-H600A5M4H, and PU/ATT-MDI-H700A3M2H nanocomposites, which were synthesized from ATT-MDI of high-, medium-, and low-grafting amounts, respectively, were inspected by TEM. TEM images (Fig. 5) of PU/ATT-MDI nanocomposites with 2.5 wt % ATT-MDI nanorods indicated that the MDI-modified ATT nanorods were dispersed in the PU matrix as bundles with diameters smaller than 100 nm in PU/ATT-MDI-H500A1M1H and PU/ATT-MDI-H600A5M4H nanocomposites (Fig. 5a and b). However, the ATT nanorods showed relatively poor dispersion in the PU/ATT-MDI-H700A3M2H nanocomposite (Fig. 5c). The superior dispersion of ATT nanorods in the PU matrix can be attributed to compatibility between the MDI-modified ATT and PU matrix. The compatibility also was confirmed by FTIR results, in which the MDI-modified ATT showed absorbance at 2275 cm−1 due to stretching of NCO groups. The NCO group is also the functional group of PU. Therefore, after the organophilic modification, the MDI-modified ATT became more compatible (or was compatiblized) with the PU matrix. This phenomenon suggests that the H700A3M2H ATT-MDI contained insufficiently modified nanorods which have affinity to cause agglomeration. The agglomeration reduced the effective surface area of the ATT-MDI and diminished the interfacial adhesion in PU/ATT-MDI-H700A3M2H nanocomposite.

Please cite this article as: M. Wong, R. Tsuji, H.J. Sue, and S. Nutt; **Glass transition temperature changes of polymer nanocomposites comprised of finely dispersed ZnO quantum dots**, Soft Matter 6 (2010) 4482-4490, DOI: http://dx.doi.org/10.1039/b927182a

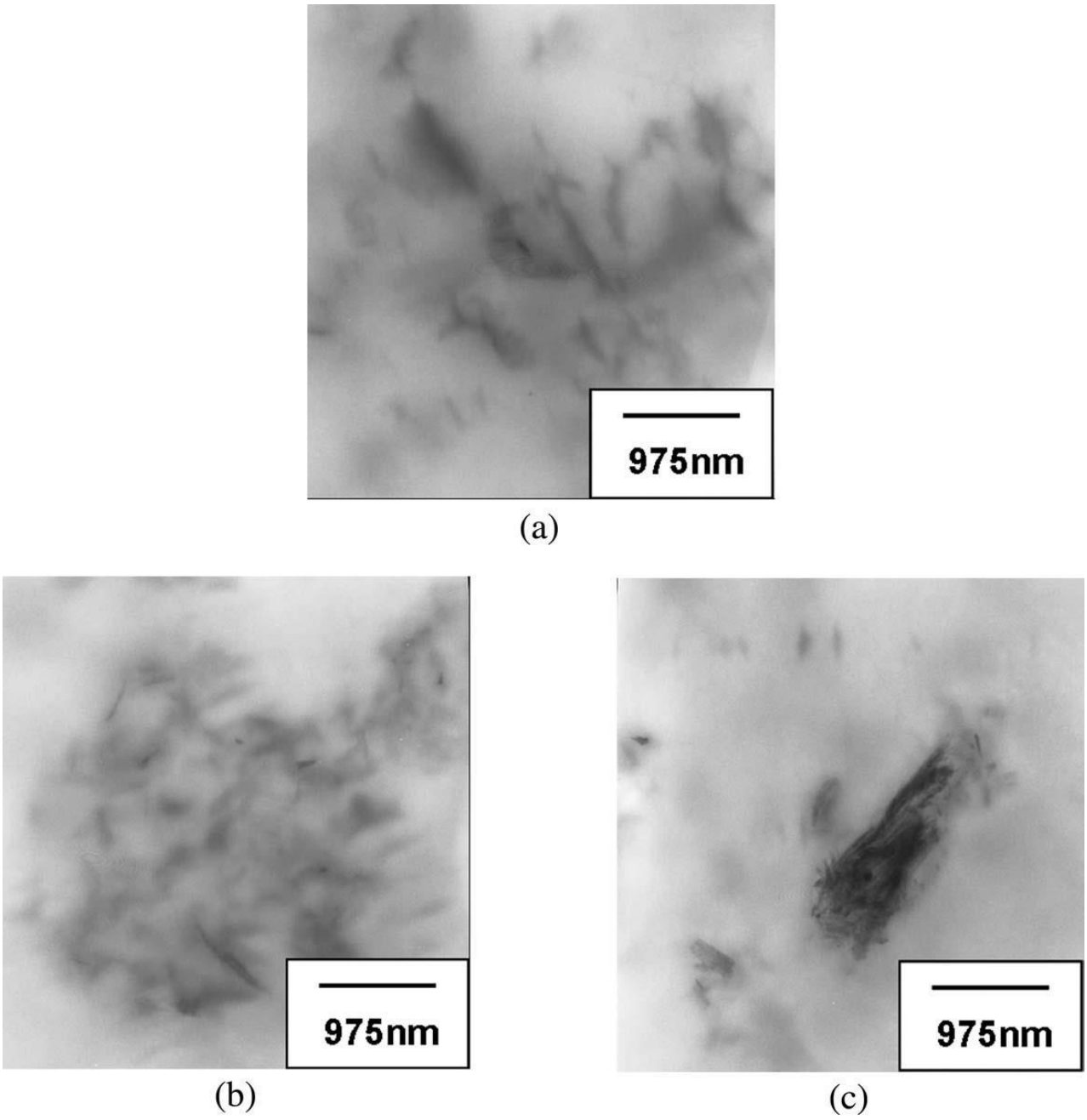

Figure 5: *TEM images of (a) PU/ATT-MDI-H500A1M1H, (b) PU/ATT-MDI-H600A5M4H, and (c) PU/ATT-MDI-H700A3M2H nanocomposites.*

Please cite this article as: M. Wong, R. Tsuji, H.J. Sue, and S. Nutt; **Glass transition temperature changes of polymer nanocomposites comprised of finely dispersed ZnO quantum dots**, Soft Matter 6 (2010) 4482-4490, DOI: http://dx.doi.org/10.1039/b927182a

3.2.2 DSC Measurements

The DSC results for neat PU and PU/ATT-MDI nanocomposites are summarized in Table 2. Because the structure of PU includes hard and soft segments, two melting temperatures are expected. However, the DSC curve (not shown) exhibited only one peak and this was associated with the melting of the soft segment (Tm, SS). The peak associated with the melting temperature of the hard segment (Tm, HS) was absent from the DSC curve [40–42]. The absence was attributed to the inactive movement of hard segment, which has a small ΔCp [43], and to the widely dispersed HS microdomains within the PU matrix [44].

Table 2: *Melting temperature and enthalpy of soft segment in PU and PU/ATT-MDI nanocomposites.*

Samples	T_m**,SS (°C)**	**Δ*H* (J/g)**
Neat PU	21.6	37.8
PU/ATT-MDI-H500A1M1H	25.84	44.98
PU/ATT-MDI-H600A5M4H	25.63	44.71
PU/ATT-MDI-H700A3M2H	25.49	44.44

The melting temperatures in the region between 21.6 and 25.84°C are characteristic of ordered soft segment structures. The values also indicate that polytetrahydrofuran crystallized in both neat PU and PU/ATT-MDI nanocomposites. For these soft segments (SS), the melting enthalpy increases from 37.8 JU/g for PU to ~44 J/g for all three PU/ATT-MDI nanocomposites. The increases in melting temperature and enthalpy of the soft segment are attributed to the effects produced by the rigid nanorods in the soft segment domains. The nanorods act as nucleation seeds, increasing the

Please cite this article as: M. Wong, R. Tsuji, H.J. Sue, and S. Nutt; **Glass transition temperature changes of polymer nanocomposites comprised of finely dispersed ZnO quantum dots**, Soft Matter 6 (2010) 4482-4490, DOI: http://dx.doi.org/10.1039/b927182a

degree of crystallinity of the PU networks. Nunes et al. [45] observed that soft segments interacted preferentially with silica, resulting in reduced interactions between soft and hard phases. In other words, the silica increased phase segregation and facilitated orientation and crystallization. In addition, the melting temperature and enthalpy of the soft segment were not significantly altered in PU/ATT-MDI-H500A1M1H, PU/ ATT-MDI-H600A5M4H, and PU/ATT-MDI-H700A3M2H nanocomposites. This suggests that the grafting content had negligible effect on the thermal behavior, although the modified ATT-MDI nanorods enhanced the crystallinity of soft segments in the PU system.

3.2.3 Dynamic Mechanical Thermal Analysis

The values of dynamic storage modulus (G′) at 50 and 100°C and, the glass transition temperature of soft segment (Tg, SS) and hard segment (Tg, HS) are summarized in Table 3. The storage modulus values at both temperatures (50 and 100°C) increased with the addition of 2.5 wt % of ATT-MDI nanorods. An increase in storage modulus of approximately 17% (over neat PU) was observed for PU/ATT-MDI-H500A1M1H nanocomposites at 50°C. However, at 100°C, the values of storage modulus for all samples dropped by roughly half, underscoring the heat sensitivity of both neat PU and PU/ATT-MDI nanocomposites within this temperature range. Despite the decrease in storage modulus values at 100°C, the G′ values for PU/ATT-MDI nanocomposites still exceeded those of neat PU. In addition, the storage modulus values for PU/ATT-MDI-H500A1M1H, PU/ATT-MDI-H600A5M4H, and PU/ATT-MDI-H700A3M2H nanocomposites at both 50 and 100°C were similar, suggesting that the dynamic mechanical thermal behavior was not strongly dependent on the grafting

Please cite this article as: M. Wong, R. Tsuji, H.J. Sue, and S. Nutt; **Glass transition temperature changes of polymer nanocomposites comprised of finely dispersed ZnO quantum dots**, Soft Matter 6 (2010) 4482-4490, DOI: http://dx.doi.org/10.1039/b927182a

amount of ATT-MDI nanorods above the melting temperature of soft segment (Table 2). The DMA data was consistent with the DSC data.

Table 3: *Storage modulus values (G') at 50 and 100°C and the peak temperatures of the tan δ curves for soft and hard segments*

Samples	***G′* (MPa) at 50°C**	***G′* (MPa) at 100°C**	**T_g, SS (°C)**	**T_g, HS (°C)**
Neat PU	21.06	10.37	−54.95	190
PU/ATT-MDI-H500A1M1H	24.54	12.21	−55.63	196.7
PU/ATT-MDI-H600A5M4H	23.83	11.96	−55.52	195.8
PU/ATT-MDI-H700A3M2H	23.63	11.86	−55.50	195.1

The glass transition temperature of soft segment (Tg, SS) and hard segment (Tg, HS) can be observed from the peaks in the tan δ versus temperature curve. The glass transition temperature values for soft segment (Tg, SS) was unchanged relative to the neat PU and PU/ATT-MDI nanocomposites. The glass transition temperature of soft segment was not influenced by the addition of nanorods or the different grafting amount of ATT-MDI. An increase in the Tg of hard segment (Tg, HS) with 2.5 wt % loading of ATT-MDI is evident in Table 3. This increase of Tg is ascribed, at least in part, to the restricted mobility of amorphous polymer chains that results from the physical crosslinks induced by crystallization, as noted by other authors [46, 47]. However, there is no obvious dependence of Tg, HS on grafting amount of ATT-MDI.

From the DSC and DMA results, we conclude that the ATT-MDI nanorods enhance crystallization in the soft segment but reduce the mobility of polymer chain in the hard segment. This can be

Please cite this article as: M. Wong, R. Tsuji, H.J. Sue, and S. Nutt; **Glass transition temperature changes of polymer nanocomposites comprised of finely dispersed ZnO quantum dots**, Soft Matter 6 (2010) 4482-4490, DOI: http://dx.doi.org/10.1039/b927182a

attributed to the heterogeneous nanorods, the enhanced interfacial adhesion to the PU matrix, and coreaction between filler and polymer.

3.2.4 Tensile Properties

The tensile yield strength, Young′s modulus, and elongation at break values for PU and PU/ATT-MDI nanocomposites are tabulated in Table 4. Compared with neat PU, the yield strength and modulus of PU/ATT-MDI nanocomposites were increased by the clay additions, although elongation at break values were decreased. Table 4 shows that the Young′s modulus and tensile yield strength of the PU/ATT-MDI-H500A1M1H nanocomposite increased by 60% and 19% respectively, whereas increases for the PU/ATT-MDI-H700A3M2H nanocomposite were more modest—38% and 0%, respectively. The PU/ATT-MDI-H500A1M1H nanocomposite resulted in the greatest yield strength and Young′s modulus values among the three PU/ATT-MDI nanocomposites, as expected, because of the highest grafting amount of MDI molecules onto the ATT-MDI nanorods. However, the values of elongation at break for PU/ATT-MDI nanocomposites were lower than neat PU and decreased with the decreasing of grafting content. In particular, the PU/ATT-MDI-H700A3M2H nanocomposite resulted in the lowest value of elongation at break. This low elongation is attributed to an insufficient amount of grafting on H700A3M2H ATT-MDI nanorods and the tendency to agglomerate in the PU matrix (Fig. 5c). This agglomeration in PU/ATT-MDI-H700A3M2H nanocomposite was responsible for the marked reduction in elongation.

Please cite this article as: M. Wong, R. Tsuji, H.J. Sue, and S. Nutt; **Glass transition temperature changes of polymer nanocomposites comprised of finely dispersed ZnO quantum dots**, Soft Matter 6 (2010) 4482-4490, DOI: http://dx.doi.org/10.1039/b927182a

Table 4: *Tensile properties of PU and PU/ATT-MDI nanocomposite*

Samples	Young's modulus (MPa)	Yield strength (MPa)	Elongation at break (%)
Neat PU	7.14	0.93	335
PU/ATT-MDI-H500A1M1H	11.4	1.11	297
PU/ATT-MDI-H600A5M4H	10.35	1.01	214
PU/ATT-MDI-H700A3M2H	9.82	0.92	177

Note that the melting point of soft segment (Tm, SS) is close to room temperature. Thus, the tensile properties at room temperature are directly related to the soft segment characteristics. Korley et al. [48] reported that the presence of crystallites within the soft segment would absorb strain energy upon deformation. Thus, semicrystalline soft segments can act as an effective load-bearing phase during deformation [48]. As shown by the DSC measurements, the ATT-MDI nanorods acted as nucleation seeds and induced crystallinity in the soft segment, resulting in an increase in the hard segment domain size and a decrease in the soft segment domain region. Consequently, the tensile yield strength and Young′s modulus of PU/ATT-MDI nanocomposites were increased, but the elongation was reduced as the crystallinity of the soft segment increased.

4. Conclusions

ATT-MDI nanorods with different grafting contents were prepared by heat and acid treatment of ATT followed by grafting with MDI. The resulting PU/ATT-MDI nanocomposites exhibited increased crystallinity and strength compared with the neat PU. These findings were attributed to

Please cite this article as: M. Wong, R. Tsuji, H.J. Sue, and S. Nutt; **Glass transition temperature changes of polymer nanocomposites comprised of finely dispersed ZnO quantum dots**, Soft Matter 6 (2010) 4482-4490, DOI: http://dx.doi.org/10.1039/b927182a

the chemical modification of ATT, especially for H500A1M1H ATT-MDI nanorods, which led to improved dispersion in the PU matrix and a strong chemical bonding between the dispersed and continuous phases. A higher grafting content on the nanorod surfaces led to more uniform dispersion and enhanced tensile properties of the nanocomposites. However, the grafting content had negligible effect on the thermal behavior of PU/ATT-MDI nanocomposites. The results demonstrate that small additions of nanorods will afford opportunities to design polymers with enhanced properties for adhesives and composite materials. Further improvements and applications in specific polymer matrices are likely to be possible with optimized surface treatments and suitable modifiers.

References

1. Y. Kojima,A. Usuki,M. Kawasumi,A. Okada,T. Kurauchi, and O. Kamigaito, J. Polym. Sci., Polym. Chem., **31**, 983 (1993).
2. Y. Kojima,A. Usuki,M. Kawasumi,A. Okada,T. Kurauchi,O. Kamigaito, and K. Kaji, J. Polym. Sci., Polym. Phys., **32**, 625 (1994).
3. Y. Kojima,A. Usuki,M. Kawasumi,A. Okada,T. Kurauchi,O. Kamigaito, and K. Kaji, J. Polym. Sci., Polym. Phys., **33**, 1039 (1995).
4. H.L. Tyan,C.M. Leu, and K.H. Wei, Chem. Mater., **13**, 222 (2001).
5. P.B. Messersmith and E.P. Giannelis, J. Polym. Sci. Part A: Polym. Chem., **33**, 1047 (1995).
6. V. Mittal, Eur. Polym. J., **43**, 3727 (2007).
7. Y.I. Tien and K.H. Wei, J. Appl. Polym. Sci., **86**, 1741 (2002).
8. K. Wang,L. Chen,M. Kotaki, and C. He, Compos. Part A: Appl. Sci. Manuf., **38**, 192 (2007).
9. B. Qi,Q.X. Zhang,M. Bannister, and Y.W. Mai, Compos. Struct., **75**, 514 (2006).
10. P. Ni,J. Li,J. Suot, and S. Li, J. Mater. Sci., **39**, 4671 (2004).
11. V.E. Yudina,J.U. Otaigbeb,S. Gladchenkoa,B.G. Olsonb,S.E. Nazarenkob,N. Korytkovac, and V.V. Gusarovc, Polymer, **48**, 130 (2007).
12. J. Vega Baudrit,M. Sibaja Ballestero,P. Vázquez,R. Torregrosa Maciá, and J.M. Martín Martínez, Int. J. Adhes. Adhes., **27**, 469 (2007).
13. S. Fakirov, Handbook of Condensation Thermoplastic Elastomers, Vol. 2, 9 (2006); Online ISBN: 9783527606610. Wiley-VCH Verlag GmbH & Co. KGaA, Weinheim.
14. J.R. Lin and L.W. Chen, J. Appl. Polym. Sci., **69**, 1563 (1998).
15. G. Oertel, Polyurethane Handbook, 2nd ed., Hanser, New York, Chapter 2, 7 (1993).
16. E. Galán and I. Carretero, Clays Clay Miner., **47**, 399 (1999).
17. E. Galan, Clay Miner., **31**, 443 (1996).
18. J.-L. Cao,G.-S. Shaoa,W. Yan,Y. Liua, and Z.-Y. Yuan, Catal. Commun., **9**, 2555 (2008).
19. N. Alexander and S. Arieh, Appl. Clay Sci., **25**, 121 (2004).
20. A. Li, and A. Wang, Eur. Polym. J., **41**, 1630 (2005).
21. L. Shen,Y. Lin,Q. Du,W. Zhong, and Y. Yang, Polymer, **46**, 5758 (2005).
22. A. Mifsud,M. Rautureau, and M. Fornes, Clay Miner., **13**, 367 (1978).

Please cite this article as: M. Wong, R. Tsuji, H.J. Sue, and S. Nutt; **Glass transition temperature changes of polymer nanocomposites comprised of finely dispersed ZnO quantum dots**, Soft Matter 6 (2010) 4482-4490, DOI: http://dx.doi.org/10.1039/b927182a

23. J. Khorami and A. Lemieux, Thermochim. Acta., **138**, 97 (1989).
24. T. Kiyohiro and R. Otsuka, Thermochim. Acta., **147**, 127 (1989).
25. U. Shuali,S. Yariv,M. Steinberg,M. Muller-Von-Moons,G. Kahr, and A. Rub, Clay Miner., **25**, 107 (1990).
26. U. Shuali,S. Yariv,M. Steinberg,M. Muller-Von-Moons,G. Kahr, and A. Rub, Clay Miner., **26**, 497 (1991).
27. R.L. Frost and Z. Ding, Thermochim. Acta., **397**, 119 (2003).
28. E. Mendelovici, Clays Clay Miner., **21**, 115 (1973).
29. M. Myriam,M. Saurez, and J.M. Martin-Pozas, Clays Clay Miner., **46**, 225 (1998).
30. M.A. Vicente-Rodríguez,J.D. Lopez-Gonzalez, and M.A. Bañares-Muñoz, Clay Miner., **29**, 361 (1994).
31. M.A. Vicente-Rodríguez,M. Suarez Barrios,J.D. Lopez-Gonzalez, and M.A. Bañares-Muñoz, Clays Clay Miner., **42**, 724 (1994).
32. M.A. Vicente-Rodríguez,M. Suarez,M.A. Bañares-Muñoz, and J.D. Lopez-Gonzalez, Spectrochim. Acta., **52**, 1685 (1996).
33. R. Yosomiya,K. Morimoto, and T. Suzuki, J. Appl. Polym. Sci., **29**, 671 (1984).
34. C.H. Wang,M.L. Auad,N.E. Marcovich, and S. Nutt, J. Appl. Polym. Sci., **109**, 2562 (2008).
35. C. Prisacariu,R.H. Olley,A.A. Caraculacu,D.C. Bassett, and C. Martin, Polymer, **44**, 5407 (2003).
36. C. Blanco,J. Herrero,S. Mendioroz, and J.A. Pajares, Clays Clay Miner., **36**, 364 (1988).
37. A. Pattanayak and S.C. Jana, Polymer, **46**, 5183 (2005).
38. A.H. Kuptsov and G.N. Zhizhin, Handbook of Fourier Transform Raman and Spectra of Polymers, Elsevier, New York (1988).
39. D.K. Chattopadhyay and K.V.S.N. Raju, Polym. Sci., **32**, 352 (2007).
40. T.A. Speckhard,K.K.S. Hwang,C.Z. Yang,W.R. Laupan, and S.L. Cooper, J. Macromol. Sci. Phys. B., **23**, 175 (1984).
41. W.J. MacKnight,M. Yang, and T. Kajiyama, Polym. Prepr. (Am. Chem. Soc., Div. Polym. Chem.), **9**, 860 (1968).
42. C.Z. Yang,K.K.S. Hwang, and S.L. Cooper, Makromol. Chem., **184**, 651 (1983).
43. I. Yilgor,J.S. Riffle,G.L. Wilkes, and J.E. Mcgrath, Polym. Bull. (Berlin), 8,535 (1982).
44. Y. Li,G. Tong,J. Liu,K. Linliu,C.R. Desper, and B. Chu, Macromolecules, **25**, 7365 (1992).
45. R.C.R. Nunes,R.A. Pereira,J.L.C. Fonseca, and M.R. Pereira, Polym. Test., **20**, 707 (2001).
46. A.P. Mathew and A. Dufresne, Biomacromolecules, **3**, 609 (2002).
47. M.L. Auad,V.S. Contos,S. Nutt,M.I. Aranguren, and N.E. Marcovich, Polym. Int., **57**, 651 (2008).
48. K. James,T. Lashanda,B.D. Pate,E.L. Thomas, and P.T. Hammond, Polymer, **47**, 3073 (2006).

Please cite this article as: M. Wong, R. Tsuji, H.J. Sue, and S. Nutt; **Glass transition temperature changes of polymer nanocomposites comprised of finely dispersed ZnO quantum dots**, Soft Matter 6 (2010) 4482-4490, DOI: http://dx.doi.org/10.1039/b927182a